International Journal of Thermophysics, Vol. 26, No. 5, September 2005 (© 2005)
DOI: 10.1007/s10765-005-8104-7

Surface Oscillations of an Electromagnetically Levitated Droplet

S. R. Berry,[1,2] R. W. Hyers,[3] L. M. Racz,[1,4] and B. Abedian[1,5]

Received January 16, 2003

The natural oscillation frequency of freely suspended liquid droplets can be related to the surface tension of the material, and the decay of oscillations to the liquid viscosity. However, the fluid flow inside the droplet must be laminar to measure viscosity with existing correlations; otherwise the damping of the oscillations is dominated by turbulent dissipation. Because no experimental method has yet been developed to visualize flow in electromagnetically levitated oscillating metal droplets, mathematical modeling can assist in predicting whether or not turbulence occurs, and under what processing conditions. In this paper, three mathematical models of the flow: (1) assuming laminar conditions, (2) using the $k-\varepsilon$ turbulence model, and (3) using the RNG turbulence model, respectively, are compared and contrasted to determine the physical characteristics of the flow. It is concluded that the RNG model is the best suited for describing this problem when the interior flow is turbulent. The goal of the presented work was to characterize internal flow in an oscillating droplet of liquid metal, and to verify the accuracy of the characterization by comparing calculated surface tension and viscosity values to available experimental results.

KEY WORDS: droplet oscillations; electromagnetic levitation; turbulence; viscosity.

[1] Department of Mechanical Engineering, Tufts University, Medford, Massachusetts 02155, U.S.A.
[2] Present Address: Lincoln Laboratory, MIT, Lexington, Massachusetts 02420-9108, U.S.A.
[3] Department of Mechanical and Industrial Engineering, University of Massachusetts, Amherst, Massachusetts 01003, U.S.A.
[4] Present Address: Energen, Inc., Lowell, Massachusetts 01854, U.S.A.
[5] To whom correspondence should be addressed. E-mail: behrouz.abedian@tufts.edu

0195-928X/05/0900-1565/0 © 2005 Springer Science+Business Media, Inc.

1. INTRODUCTION

1.1. Measuring Thermophysical Properties Using Oscillating Droplets

The oscillating drop method is a technique used for measuring thermophysical properties of liquid conductive materials, such as surface tension and viscosity. It is especially useful for highly reactive or undercooled metals, since the process is containerless and the sample can be kept very pure or in a metastable state for the duration of the experiment. The sample, usually weighing approximately 1 g, is levitated in an electromagnetic field, which is generated by an alternating current flowing through an axisymmetric water-cooled copper coil. The coil must be designed appropriately so that the sample levitates in a stable manner. Brooks and coworkers [1] have recently summarized the merits of thermophysical property measurements using this technique.

1.2. Theory: Oscillating Droplets in Electromagnetic Levitation

When a conductive sample is positioned inside an alternating magnetic field **B**, an eddy current is induced within the sample. Associated with this induced current is (1) Joule heating through Ohmic losses, which can be used to heat and melt the material, and (2) a magnetic force known as the Lorentz force F,

$$F = \tfrac{1}{2}\Re\left(J \times B^*\right) \tag{1}$$

where J is the induced current density, $\Re$ denotes the real portion of the complex quantity, and $(^*)$ denotes the complex conjugate part of the magnetic field B. The Lorentz force provides the lifting force on the sample and induces internal fluid flow if the sample is molten.

When the surface of a molten droplet is subjected to a deforming force and subsequently released, it experiences a restoring mechanism that manifests itself as oscillations about the equilibrium shape of the droplet. Viscosity and surface tension can be measured by detecting and analyzing these oscillations; surface tension is related to frequency, and viscosity is related to damping. The radius of a viscous spherical droplet undergoes damped oscillations of the form,

$$R_{n,m}(\theta, \phi, t) = \cos\left(2\pi \nu_{n,m} t e^{-\Lambda_{n,m} t} P_n^m \cos\theta\right) \cos\left(m\left(\phi - \phi_o\right)\right) \tag{2}$$

where n is the index of the fundamental oscillation modes, m is the index of one of the $(2n-1)$ possible modes, where $|m| \le n$, θ is the angle with respect to the axis of symmetry, ϕ is the azimuthal angle, $\nu_{n,m}$ and $\Lambda_{n,m}$ are the frequency and damping constant, respectively, for the given mode,

P_n^m is a Legendre function, and ϕ_o is an arbitrary symmetry direction. The oscillation mode $n=2$ is the first that can reveal fluid properties of the sample. The $n=2$, $m=0$ mode is symmetric about the z-axis, and is the only one observed for a well-behaved axisymmetric droplet excited by an axisymmetric electromagnetic force, as is the case in experiments designed for determination of thermophysical properties.

Lord Rayleigh determined the relationship between surface tension γ and oscillation frequency for small deformations of an inviscid liquid sphere as [2]

$$\omega_n^2 = \frac{n(n-1)(n+2)\gamma}{\rho R^3} \tag{3}$$

where ω_n is the angular frequency of the oscillation mode n for a droplet having mass density ρ and radius R. Corrections must be made to the Rayleigh frequency in order to take into account the effects of finite viscosity, magnetic field, and gravity. Viscosity-related corrections are addressed by Suryanarayana and Bayazitoglu [3], and gravity and magnetic field-related corrections are treated by Cummings and Blackburn [4]. Instead of full-scale numerical calculations for the freely oscillating drop presented in this paper, Meradji et al. [5] recently used a Galerkin/finite element technique along with the spine method for interfacial deformations to solve for the fluid flow inside a drop under zero gravity. This approach is restricted to laminar flow conditions, can handle only regular droplet deformations, and is not computationally efficient.

Lamb determined the relationship between the viscosity μ and damping of the oscillations as [6]

$$\tau_n = \frac{\rho R^2}{(n-1)(2n+1)\mu} \tag{4}$$

where τ_n is the damping constant for fundamental oscillation mode n. There are a number of practical limitations for use of this equation. Viscosity cannot be determined by electromagnetic levitation experiments performed on earth under $1-g$ because droplet oscillation does not attenuate because of the applied Lorenz force; the experiments can be performed in space under microgravity where minimal levitation force is necessary to keep the drop suspended. Furthermore, Eq. (4) gives an accurate value of molecular viscosity only if the flow in the droplet is laminar. If the flow is transitional or turbulent, an effective viscosity μ_{eff} is obtained, which is the sum of the molecular viscosity μ and a turbulent eddy viscosity μ_{T}. The turbulent eddy viscosity represents an additional resistance to flow caused by the swirling of eddies in a turbulent flow field. Currently, the only means of determining accurate molecular viscosity values by the oscillating drop method is by performing measurements

using different combinations of experimental parameters, inducing different levels of fluid flow. Measured values that are independent of these parameters are considered valid.

The experimental complexity of oscillating drop viscosity measurements could be reduced considerably if a reliable means of obtaining detailed knowledge about transition and turbulence in levitated droplets were available. This work represents a step toward this goal.

1.3. Modeling Turbulence in EML

Turbulence modeling in levitated droplet systems has been limited. Prior work falls into three categories: assumed laminar flow, assumed constant eddy viscosity (which corresponds to fully developed, isotropic turbulence), and the $k-\varepsilon$ model. These works are adequately reviewed elsewhere [7, 8].

In previous work [8], the authors performed an analysis to show that μ_T in electromagnetically levitated spherical droplets must be *non-uniform*, and compared the renormalization group (RNG) [9] and $k-\varepsilon$ and turbulence models' ability to generate physically reasonable distributions of turbulent eddy viscosity. The analysis did not take into account possible contributions to turbulence by the droplet oscillations. The present work relaxes the assumption of non-deforming droplets and extends the turbulence study to oscillating droplets.

2. TURBULENCE MODELING

In this work, we use two well-known approaches, $k-\varepsilon$ and RNG, to model turbulence in a levitated droplet. These turbulence models have been used extensively in other flow geometries and will be used here for the sake of comparison and for confirmation of physical principles governing the flow. In the $k-\varepsilon$ approach, turbulent viscosity ν_T is estimated locally via calculations of the turbulent kinetic energy k and the turbulent rate of dissipation ε. There are two additional transport equations to be solved for k and ε, which contain five empirical constants. These constants are assumed to be universal and geometry-independent. $k-\varepsilon$ is by far the most widely used turbulence model, however, its inadequacies are well documented [10].

Among the new alternatives to $k-\varepsilon$ is the renormalization group (RNG) algorithm first proposed by Yakhot and Orszag [9]. In this procedure, the dynamic equations for the ensemble-averaged velocity field are derived by averaging over an infinitesimal band of small-scale fluctuations in order to remove them from explicit consideration. The influence of

these small scales is only manifested in the larger-scale dynamics through a change in the effective viscosity μ_{eff}. A Gaussian forcing function is used to incorporate the effects of large eddies in the inertial range. Modification of the effective viscosity by statistical elimination of smaller scales is an iterative and cumulative process known as coarse graining that continues until the viscosity becomes scale independent. There are a number of different implementations of the RNG method. The one used in this study is referred to as "RNG $k-\varepsilon$", because RNG expansions are used to obtain the constants in the transport equations for k and ε. This technique has been shown to be effective in swirling flows, stagnation flows, relaminarizing flows, and low Reynolds number and transitional flows.

3. MODEL DEVELOPMENT

3.1. Goals and Scope

In this work, we focus on a test case; a nickel droplet levitated under microgravity conditions in TEMPUS, *Tiegelfreies Elektro-Magnetisches Prozessieren Unter Schwerelosigkeit* (Containerless Electro-Magnetic Processing under Weightlessness), a facility designed for international microgravity studies. Our goal is to develop a turbulence model that accurately predicts the physical characteristics of the flow in the nickel droplet when it is subjected to two different force fields; these fields correspond to those generated by the TEMPUS facility. Because there are no experimental data available that show the structure of the flow inside the droplet, we verify our results indirectly, by comparing with known physical principles, other numerical models, and experimental oscillation frequency and damping.

In developing our model, we have considered that there may be two contributions to turbulence. The first is due to the electromagnetic field, which penetrates into the droplet to a distance of the skin depth δ. Strong body force gradients adjacent to the free surface give rise to fluid flow and stress variations, which may give rise to the production of turbulence. The second contribution to turbulence production may be strong free surface oscillation of the droplet. In this work, we take both into account.

3.2. Electromagnetic Calculations

The purpose of the electromagnetic calculations is to determine the free surface shape of the droplet and to determine the spatial distribution of the Lorentz force $\mathbf{F}$ for use as a body force term in the governing equations of fluid flow. We assume that the droplet is isothermal. We use the method of mutual inductances [11] to solve the magnetoquasistatic form of Maxwell's equations. Because of the high frequency of electromagnetic

oscillations, the magnetic induction is independent of the velocity field in the droplet; and in turn, the fluid reacts to only the real portion of the electromagnetic force.

The two force distributions generated by the TEMPUS coils are shown in Figs. 1 and 2. A schematic diagram of the coils is shown in Fig. 3. The coils are cylindrical in shape and are controlled by two separate radio-frequency circuits, which allow for independent heating and positioning of a sample. The force distribution shown in Fig. 1 is the positioner field, used to hold the droplet in a stable manner during an experiment. The maximum force generated by this field is 7.33×10^4 $\mathrm{N \cdot m^{-3}}$, applied at the surface of the droplet at $\pm 49.5^\circ$ from the equator. The force field shown in Fig. 2 represents the superposition of the positioner field and a heater field, used to heat and melt samples and also to induce oscillation for viscosity and surface tension measurements. The maximum force generated by this combined field is 1.04×10^6 $\mathrm{N \cdot m^{-1}}$, applied on the surface of the droplet at the equator. A superposition of the positioner and heater fields is dominated by the heater field. The two force fields were used as F in the laminar and turbulent Navier–Stokes equations, Eqs. (5) and (6), respectively, in computing internal fluid flow;

$$\frac{\partial u}{\partial t} + (u \cdot \nabla)\, u = -\frac{1}{\rho}\,(\nabla p + F) + \nu \nabla^2 u \tag{5}$$

$$\frac{\partial \overline{u}}{\partial t} + (\overline{u} \cdot \nabla)\, \overline{u} = -\frac{1}{\rho}\,(\nabla \overline{p} + F) + \nabla\,(\nu + \nu_T)\,\nabla \overline{u} \tag{6}$$

It should be noted that the body force F has a strong rotational component that contributes to vorticity production in the droplet. $\nabla \times F$ in the magnetized region of the fluid is of order F/δ, with δ being the depth of penetration of F below the free surface known at the skin depth. The two force field distributions in Figs. 1 and 2 are such that δ is roughly 10% of the droplet radius in our calculations.

3.3. Fluid Flow Calculations

The multiphase volume-of-fluid (VOF) method was used to represent the free surface of the levitating droplet. This model tracks the interface between two or more immiscible fluids across cell boundaries in a fixed structured mesh [12]. The Eulerian approach is used to determine the position of the free surface by solving the continuity equation for volume fractions of the fluids in the flow domain. In our calculations, two fluids were defined; Fluid 1 was assigned the thermophysical properties of nickel at its melting point representing the droplet, and Fluid 2 was

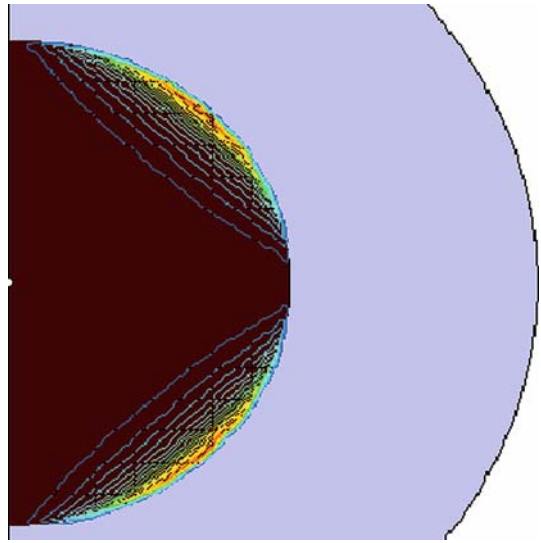

Fig. 1. Positioner force field used in TEMPUS experiments. Force contours are at 3.86×10^3 N · m^{-3} increments from 0.0 to a maximum of 7.33×10^4 N · m^{-3} at the free surface.

assigned the thermophysical properties of air, representing the region surrounding the droplet. Because phase changes and microstructural evolution within the sample are not simulated, the surrounding fluid need not be identical to the actual gas used in the experiments. The purpose of Fluid 2 is to ensure a distinct boundary (free surface) between the two fluids. The penalty for using the VOF model to represent a free surface is unnecessary computation in Fluid 2, lengthening the overall computation time. Because of the axisymmetric body force fields, modeling one quadrant of the droplet would have been sufficient for this study. However, we used a hemispherical grid in order to have the capability to model ground-based levitation systems, in which droplet flow fields show no symmetry about the equator.

The electromagnetic forces were imposed on the computational domain by means of a subroutine, in which forces were assigned at discrete grid locations. For a deforming droplet, the force is acting relative to the free surface exposed to an external electromagnetic field. Because the grid itself does not deform, another subroutine was used to enable the forces to track the moving free surface of the oscillating droplet [13]. Through dimensional analysis, we determined that a semi-coupled model

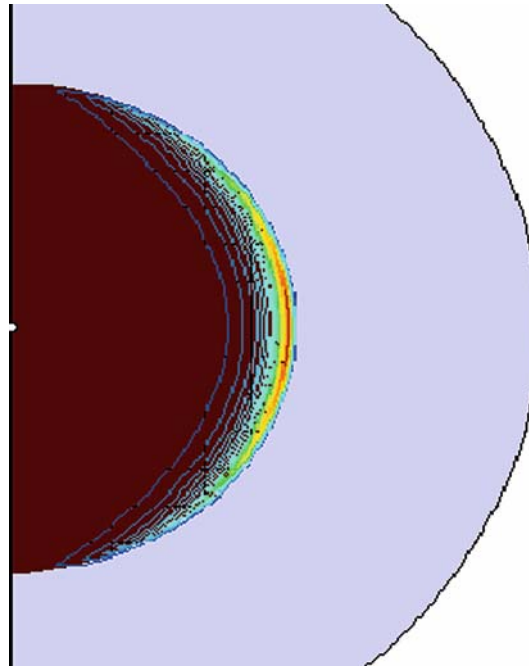

Fig. 2. Heater plus positioner force fields in THEMPUS experiments. Force contours are at 3.59×10^4 N · m^{-3} increments from 0.0 to a maximum of 1.04×10^6 N · m^{-3} at the free surface.

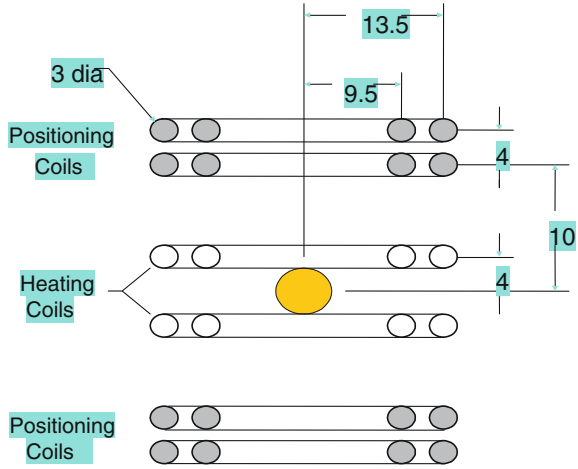

Fig. 3. Schematics of TEMPUS levitation coils. Lengths are in mm.

is appropriate [8], in which the magnetic calculations are performed neglecting the effects of fluid flow. Three-dimensional swirling effects were also neglected, justified by the assumption that an axisymmetric droplet and a symmetric force field yield an axisymmetric time-averaged velocity profile.

Time-dependent flow simulations were performed using Fluent, a commercial computational fluid dynamics package. We invoked a laminar model, followed by the $k-\varepsilon$ and RNG turbulence models. The positioner field simulations continued until the solution reached steady state, or asymptotic behavior. Then the heating field was applied for 100 ms, the length of time for which heating pulses were applied to droplets in the TEMPUS facility in order to induce droplet oscillation. Therefore, after its initial application, the heater field is relaxed and the droplet exposed to the positioner field alone. The shutting off of the heater field sets the droplet into oscillations. The frequency and rate of attenuation of the calculated oscillations was recorded. After performing appropriate grid sensitivity analysis, we used a 60×60 grid (within Fluid 1) for all calculations.

4. RESULTS AND DISCUSSION

4.1. Results

The maximum flow velocities upon application of the heater and positioner force fields, calculated by the laminar, RNG, and $k-\varepsilon$ models may be found in Table I. Figure 4 shows the velocity profiles for the positioner field, and Fig. 5 shows effective viscosity results for the positioner field. Figures 6 and 7 show results obtained upon application of the heater field. Finally, Fig. 8 represents the computed surface oscillations obtained after the heater was applied for 100 ms and removed, with a superimposed curve fit to show the exponential decay.

Table I. Maximum Velocity Magnitude ($m \cdot s^{-1}$) Calculated for the Force Field Distributions and the Computational Models.

	Positioning	Heating
Laminar	0.06	0.43
RNG	0.02	0.1
$k-\varepsilon$	0.004	0.05

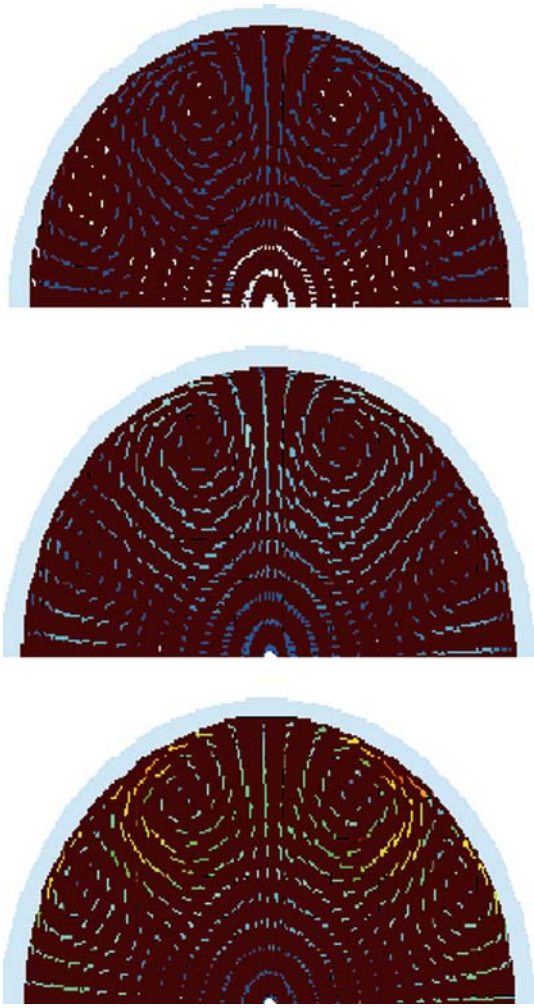

Fig. 4. Flow patterns in the deforming droplet generated by the positioning force for $k-\varepsilon$, RNG and purely laminar models, top to bottom, respectively.

4.2. Discussion

The data in Table I show that the maximum velocities are different for each of the three models examined. The difference may be accounted for by the method with which the turbulent eddy viscosity is generated by the different algorithms. In the laminar model, there is no turbulent model

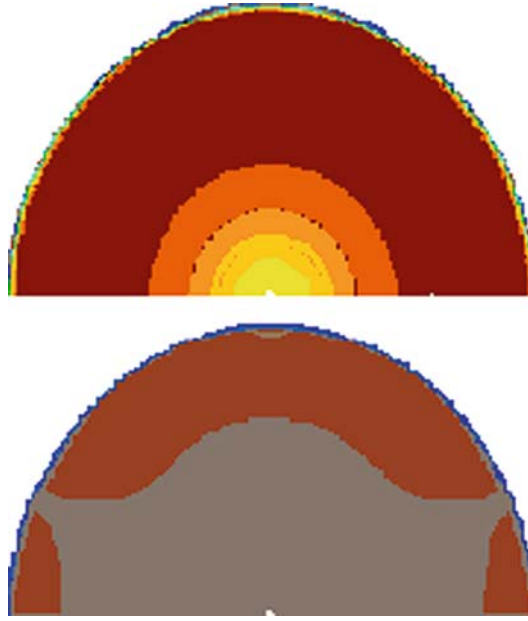

Fig. 5. Effective viscosity contours for $k-\varepsilon$ and RNG models for the positioner field, top to bottom, respectively.

or turbulent eddy viscosity. The flow is damped by molecular viscosity only, resulting in the highest velocities of the three calculations. At the other extreme lies $k-\varepsilon$, which predicts the lowest maximum velocity. The reason for this is that in the $k-\varepsilon$ method, constant length and velocity scales are assumed throughout the computational domain, resulting in an isotropic representation of turbulent eddy viscosity. Such a representation works well for many high Reynolds number flows, but flows involving curvature, rotation, and vortices are not well represented, nor are many low Reynolds number turbulent flows [13]. In contrast, the RNG method allows for different length and velocity scales in the flow, resulting in a more physical description of turbulent eddy viscosity. We have shown in previous work that an accurate representation of the droplet would show turbulence generation in areas where the flow is undergoing rapid deceleration or an abrupt change in direction, and no turbulence generation at axes or points of symmetry, or at the free surface, where the shear is zero [8]. The maximum velocity value obtained by the RNG method is consistent with this analysis. Further information can be gleaned from the velocity and effective viscosity plots in Figs. 4 through 7. Figure 4 shows that

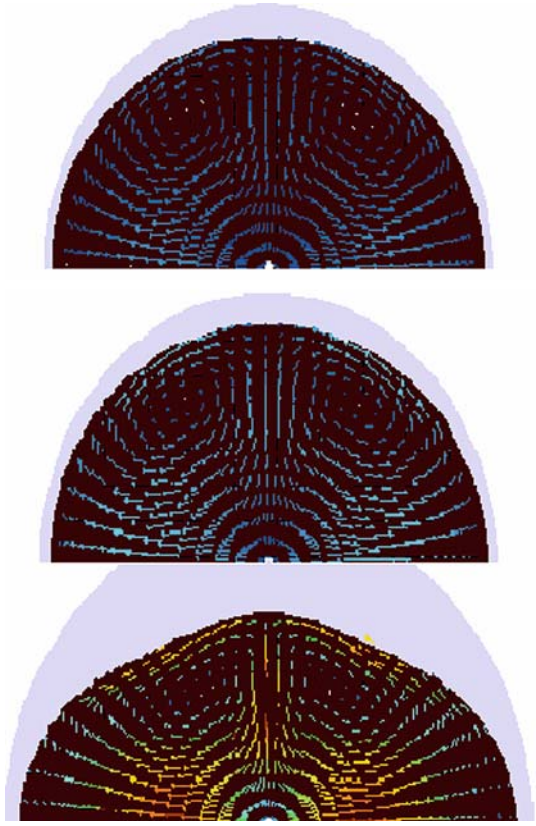

Fig. 6. Flow patterns in the deforming droplet generated by the combined heating and positioning forces for $k-\varepsilon$, RNG, and purely laminar models, top to bottom, respectively.

all of the models produce qualitatively very similar velocity profiles; the discrepancies become apparent on the effective viscosity plots in Fig. 5. The RNG model has calculated the highest effective viscosity at the equator of the droplet (top of the figure), where the greatest deceleration and change in flow direction takes place. It has also calculated relatively higher values near two recirculation loops, while the lowest values are in the center of the droplet. These results are physically reasonable. In contrast, the $k-\varepsilon$ results show little relationship to the physical nature of the flow. The highest effective viscosity values have been calculated in the droplet center, and the values are only a function of radius throughout.

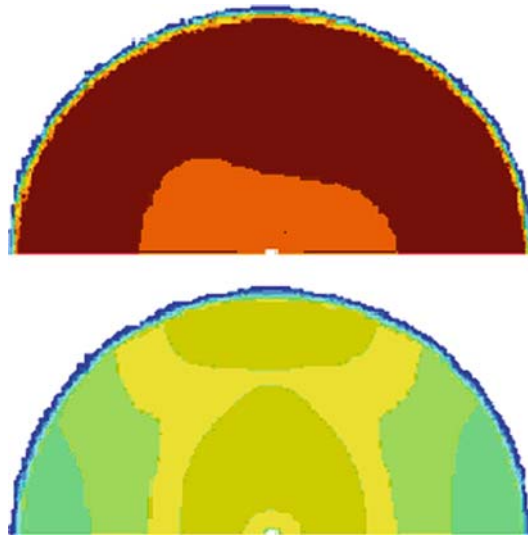

Fig. 7. Effective viscosity contours for $k-\varepsilon$ and RNG models for the combined heating and positioning forces, top to bottom, respectively.

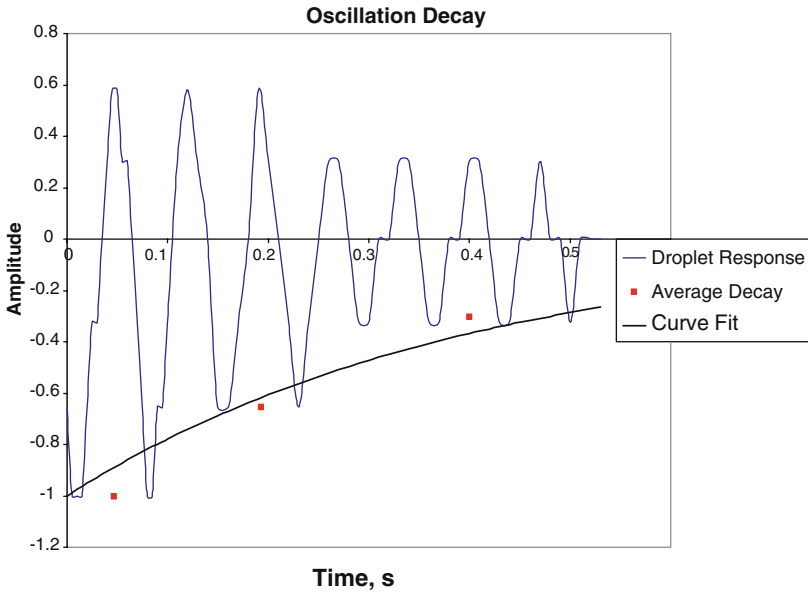

Fig. 8. Calculated surface oscillations of nickel droplet after removal of the heater field.

When the heater field is applied for 100 ms, our calculations indicate that the flow is turbulent. The laminar model yields far too high velocities and an unreasonably large droplet deformation. In contrast, the RNG and $k-\varepsilon$ models calculate qualitatively similar results and an average effective viscosity high enough to prevent excessive droplet deformation. The prediction that there is some turbulence in the droplet agrees with experimentally observed deformation of liquid nickel. The effective viscosity plots for the heater field show the difference between the $k-\varepsilon$ and RNG results. The $k-\varepsilon$ model does not yield physical results, even ignoring the asymmetry, which has occurred in the converged result. The RNG model once again shows azimuthal as well as radial variations in the effective viscosity, with the highest values occurring in the region of greatest deceleration and greatest change in flow direction.

Overall, the results may be interpreted as follows; the RNG algorithm is more successful in describing turbulent flow with laminar regions than is the $k-\varepsilon$ algorithm. The more turbulent the flow, the better results the $k-\varepsilon$ model generates. In geometries in which symmetry prescribes that turbulent eddy viscosity be non-uniform, RNG-based methods are preferable.

It is readily apparent from this work that the turbulence field inside the droplet is highly non-homogeneous. Upon removal of the electromagnetic force, it also becomes non-stationary, as turbulence diffuses from areas of high intensity to areas of low intensity. RNG-based simulations have shown that this diffusion occurs on a time scale of milliseconds consistent with the diffusion time scales based on local eddy diffusion. After these first few milliseconds, during which time the kinetic energy of the flow decays, the turbulent areas lose their intensity and the quiescent areas begin to advance within the flow domain. An overall decay in velocity due to viscous dissipation attenuates the oscillation amplitude.

Figure 8 shows that the calculated droplet oscillations behave in a qualitatively correct manner, in that the period of oscillations is constant and the oscillations decay exponentially with time. The period of oscillations was found to be 70 ms. Using the Rayleigh formula, this results in a surface tension value of 0.51 $\mathrm{N \cdot m^{-1}}$, which is approximately 70% too small. The corrections mentioned in Section 1.2 were not applied, but as they account for only a few percent under microgravity conditions [14], their absence does not explain the large discrepancy. It is also clear that the fluid flow calculations themselves are not responsible for the large error, because oscillation frequency is largely independent of fluid flow. The VOF model is likely to be primarily responsible, specifically the algorithm that determines the response and direction of motion of the droplet free surface. A solver in which the dynamics of free surfaces are handled by more sophisticated algorithms is expected to yield more accurate results.

The curve that represents the rate of decay has the form

$$A(t) = A_0 e^{-t/\tau_n} \tag{7}$$

where τ_n is the decay constant. The best fit for τ_n is 0.04 s. Using Lamb's formula (Eq. (4)) and the decay constant from the curve fit, a viscosity value was calculated to be 0.06 Pa · s, which is twelve times the molecular viscosity value.

It is important to understand that the decay constant was found immediately after the heater field was removed. Our results show that the internal fluid flow generated is turbulent at this time. Lamb's formula does not account for turbulence, but the result can be corrected to obtain a molecular viscosity. We rewrite Lamb's formula solved for the effective viscosity:

$$\bar{\mu}_{\text{eff}} = \frac{\rho R^2}{(n-1)(2n+1)\tau_n} \tag{8}$$

where $\overline{\mu}_{\text{eff}}$ represents the spatial average effective viscosity. $\overline{\mu}_{\text{eff}}$ can be broken down further into $\mu + \overline{\mu}_{\text{T}}$, where $\overline{\mu}_{\text{T}}$ represents the spatial-average turbulent eddy viscosity.

The reported numerical experiments on an oscillating nickel droplet shed new light on previous experimental attempts to measure viscosity from the damping of oscillations. During the IML-2 (Second Microgravity Science Laboratory) mission of the Space Shuttle (STS-65, July 1994), the viscosity of gold was obtained from the damping constant that was 13 times the proper atomic value [15]. The same discrepancy was also observed for an AuCu sample. The presented numerical results in this paper indicate that turbulence in the molten droplet was the dominant damping mechanism in these experiments.

These results also demonstrate the importance of understanding the transition to turbulence in EML, including a criterion for determining *a priori* whether a given combination of operational and materials parameters will result in laminar or turbulent flow. Such an understanding will enable the proper choice of parameters to ensure laminar flow for oscillation measurements. Laminar-turbulent transition of MHD flow inside a levitated PDSI droplet has been observed by Hyers et al. [7], and there are recent analytical developments of flow instabilities for spherical droplets [16]. However, these studies are still in early stages of their development and are concerned only with non-deforming droplets. We expect computational calculations will remain an important part of future space missions.

This recommended procedure must be refined further, as we did not recover the exact input surface tension value, as we should have in the

absence of temperature effects. The discrepancy may be indicative that the VOF model is responsible for aberrant surface behavior. Therefore, more robust free surface modeling is recommended in future calculations.

5. CONCLUSIONS

(a) Fully time-dependent calculations of the flow field inside an electromagnetically levitated oscillating nickel droplet were successfully performed. Flow fields obtained by three different models; laminar, $k-\varepsilon$ and RNG, were compared in order to assess the reliability and applicability of each of the results.

(b) The results, in particular those describing turbulent eddy viscosity, indicate that the RNG method is superior to $k-\varepsilon$ in describing turbulent flow in this problem, and potentially, the analysis of all problems involving low Reynolds number turbulent flow, recirculating flow, relaminarizing flow, and/or free surface flow. Other alternatives to $k-\varepsilon$ are being continuously developed. They should also be examined in detail.

(c) These models predict a sufficient level of turbulence to have a strong effect on the damping of surface oscillations in the droplets. For the case of a droplet in TEMPUS, the turbulence causes the surface oscillations to damp 12 times faster than viscosity alone; this prediction agrees remarkably with the observed value of 13 times faster damping for a gold drop [15]. These results highlight the importance of obtaining laminar flow and understanding the onset of turbulence as a pre-condition for such measurements.

(d) Many questions still remain regarding flow in electromagnetically levitated droplets, despite the popularity of oscillating droplet techniques in materials science and materials processing. In particular, there has been no flow visualization performed on these systems to date. Such experiments are required in order to ascertain whether the fluid mechanics are understood. An important question pertains to the transition to turbulence, at present a stumbling block in most levitated droplet modeling efforts.

REFERENCES

1. R. F. Brooks, I. Egry, S. Seetharaman, and D. Grant, *High Temp. - High Press.* **33**:631 (2001).
2. J. W. S. Rayleigh, *Proc. Royal Soc. London*. **29**:71 (1879).
3. P. V. R Suryanarayana and Y. Bayazitoglu, *Phys. Fluids A* **3**:967 (1991).

4. D. L. Cummings and D. A. Blackburn, *J. Fluid Mech*. **224**:395 (1991).
5. S. Meradji, T. P. Lyubimova, D. V. Lyubimov, and B. Roux, *Cryst. Res. Technol*. **36**:729 (2001).
6. H. Lamb, *Proc. London Math. Soc.* **13**:51 (1881).
7. R. W. Hyers, G. Trapaga, and B. Abedian, *Met. Trans. B* **34**:29 (2003).
8. S. R. Berry, R. W. Hyers, B. Abedian, and L. M. Racz, *Met. Trans. B* **31**:171 (2000).
9. V. Yakhot and S. A. Orszag, *J. Sci. Comp*. **1**:1 (1986).
10. W. Rodi. *Turbulence Models and their Applications in Hydraulics* (Brookfield Publishing, Philadelphia, 1984).
11. J.-H. Zong, J. Szekely, and E. Schwartz, *IEEE Trans. Magn.* **28**:1833 (1992).
12. C. W. Hirt and B. D. Nichols, *J. Comp. Phys.* **39**:210 (1981).
13. S. R. Berry, *M.S. Thesis* (Tufts University, Medford, Massachusetts, 1998).
14. R. W. Hyers, G. Trapaga, and M. C. Flemings, *Solidification 1999* (TMS, Warrendale, Pennsylvania, 1999), pp. 23–31.
15. Team TEMPUS, "Materials and Fluids under Low Gravity," *Proc. IXth Eur. Symp. on Gravity-Dependent Phenomena in Phys. Sci., Lecture Notes in Physics 464* (Springer, New York, 1996), pp. 233–252.
16. V. Shatrov, J. Priede, and G. Gerbeth, *Phys. Fluids* **15**:668 (2003).